CHINESE OPTICS LETTERS

Vol. 23, No. 1 | January 2025

Stable cascaded femtosecond optical parametric amplifiers in the NIR-I region at 50 MHz

Xiaoxuan Zhu (朱晓璇), Jue Wang (王 珏), Xuechen Gao (高雪晨), Jintao Fan (范锦涛)*, and Minglie Hu (胡明列)**

Ultrafast Laser Laboratory, Key Laboratory of Opto-electronic Information Technical Science of Ministry of Education, School of Precision Instruments and Opto-electronics Engineering, Tianjin University, Tianjin 300072, China

*Corresponding author: fanjintao@tju.edu.cn

**Corresponding author: huminglie@tju.edu.cn

Received June 28, 2024 | Accepted July 31, 2024 | Posted Online February 5, 2025

We experimentally demonstrate a continuous-wave (CW) injection-seeded cascaded optical parametric amplifier (OPA) for generating femtosecond pulses in the NIR-I spectral region. Utilizing a cascaded two-stage configuration, our system achieves an output of 347 mW of NIR radiation centered at 792 nm, combined with a pulse duration of 171 fs at a repetition rate of 50 MHz. The CW seeding intrinsically ensures superior pulse-to-pulse and long-term power stability. Our measurements indicate a relative intensity noise (RIN) of 2.2% root mean square (RMS) (integrated from 3.3 Hz to 2.5 MHz) and an RMS power stability as low as 0.63% over a duration of 90 min. Moreover, the beam quality of the output beam is near-diffraction-limited, with M^2 factors of M_X^2 = 1.11 and M_Y^2 = 1.29. We believe that this type of laser source is capable of delivering stable femtosecond pulses within the NIR-I spectral range and can serve as an ideal solution for various applications including biophotonics, microscopy, and laser processing.

Keywords: continuous-wave injection; cascaded optical parametric amplifier; superior power stability; high beam quality.
DOI: 10.3788/COL202523.011902

1. Introduction

Femtosecond laser sources in the NIR-I (700–900 nm) spectral region have emerged as invaluable tools, for a variety of applications including biophotonics[1], spectroscopy[2], microlens array fabrication[3], and microelectronic device manufacturing[4]. In particular, such emission systems with a repetition rate in the range of several tens of megahertz are of great interest to those research communities that require high signal-to-noise ratio, large statistics, and high flux[5]. In this regard, Kerr-lens mode-locked (KLM) Ti:sapphire lasers oscillators, renowned for providing the shortest pulses with only 5 fs duration directly from the oscillator[6,7], continue to serve as the primary workhorse in the research field due to the remarkable spectral bandwidth of this gain material. Nevertheless, these systems suffer limitations in terms of power scaling primarily due to the inevitable heat load within the laser crystal. Additionally, these laser sources, often pumped by Argon-ion lasers[8] or frequency-doubled diode-pumped solid-state lasers[9], contribute to increased volume and cost in Ti:sapphire lasers.

As an alternative, femtosecond optical parametric oscillators (OPOs) synchronously pumped by the second-harmonic generation (SHG) from Yb-fiber amplifiers or high-power bulk oscillators, provide a compelling laser source in the NIR-I spectral region. In contrast to Ti:Sapphire lasers, OPOs rely on a second-order nonlinear conversion process, rendering them impervious to the effects of gain heat accumulation. As a result, based on such OPOs, watt-level output power combined with sub-50 fs pulse duration can be produced. In 2017, Coluccelli *et al.* reported a watt-level femtosecond OPO based on barium borate (BBO) pumped by a frequency-doubled Yb-fiber laser, providing a signal tuning of over 680–910 nm with a minimal pulse duration of 30 fs at 740 nm[10]. However, in terms of the synchronous pumping condition, the cavity length of the OPO must precisely match that of the pump, typically spanning several meters[11–13], thereby augmenting the resonator's volume. Furthermore, the output wavelength is quite sensitive to the detuning of the cavity length. Hence, to maintain both the output power and the operational wavelength, the implementation of an active stabilization scheme is imperative[14,15].

Compared with OPOs, optical parametric amplifiers (OPAs) feature the advantages of not requiring a synchronous cavity. This not only greatly reduces the physical size of the system but also can achieve a stable output without any feedback loop. In the NIR-I spectral region, OPAs typically rely on seed sources generated by white light continuum (WLC) radiation[16–19]. Meeting this requirement necessitates several micro- to millijoules of pulse energy for the pump laser source, thereby

constraining the laser to repetition rates of several kilohertz. As the repetition rate of the pump laser reaches tens of megahertz, achieving the necessary peak power to drive the nonlinear effects becomes increasingly challenging. On the other hand, continuous-wave (CW) injection-seeded OPAs have demonstrated excellent noise performance and phase stability at the nanojoules level pump with an operating repetition rate of tens of megahertz[20]. This type of OPA has achieved great success in both telecommunication[21] and the mid-infrared (MIR) spectral region[22]. However, to the best of our knowledge, such an OPA system has not been previously realized in the NIR-I region. Although periodically poled $LiNbO_3$ (PPLN), lithium triborate (LBO), and BBO have been available for a long while, they face challenges in directly generating NIR radiation at tens of megahertz repetition rates. While PPLN crystals have superior nonlinear coefficients, generating NIR wavelengths requires green light as the pump, which often damages the coating, making them unsuitable for green-pumped OPA systems. On the other hand, LBO and BBO crystals have limited nonlinear coefficients and typically require pump laser sources with pulse energies in the micro- to milli-joule range. These OPAs are usually pumped by laser systems with repetition rates of several kilohertz. However, achieving the necessary peak power for driving the nonlinear effects becomes challenging when the pump laser's repetition rate reaches tens of megahertz.

In this Letter, we propose and experimentally demonstrate a cascaded CW injection-seeded femtosecond OPA system to deliver high-repetition rate femtosecond pulses in the NIR-I region. In the first stage, the 1480 nm CW seed is amplified by the fundamental output of a Yb-doped fiber laser. Subsequently, in the second stage, the amplified 1480 nm pulses are defined as the idler of the OPA and are further amplified by the frequency-doubled green light. Thanks to nonlinear frequency conversion, the second-stage signal is free from the CW background. The maximum power of 347 mW and the pulse duration of 171 fs are obtained at 792 nm (signal) with an M^2 value of 1.11×1.29. Benefitting from the initial CW seed laser source, this cascaded OPA exhibits a long-term stability output of 0.63% root mean square (RMS) over 90 min and a relative intensity noise (RIN) of 2.2% RMS (integrated from 3.3 Hz to 2.5 MHz).

2. Experiment and Setup

The experimental configuration consists of two OPA stages and an SHG module, as illustrated in Fig. 1. The cascaded OPA system is pumped by a femtosecond laser system (BFL-1030-10LEW), which emits pulses with a duration of 219 fs and a central wavelength of 1030 nm. The laser source operates at a repetition rate of 50 MHz, delivering a maximum pump power of up to 15 W. The laser pulses are sent into the cascaded OPA system, with the initial pump power of 10.86 W to ensure that the energy is under the laser-induced damage threshold of the crystals. To finely manipulate the energy distribution between the two optical paths, a polarization beam splitter (PBS) is coupled with a half-wave plate (HWP2), serving as the power controller.

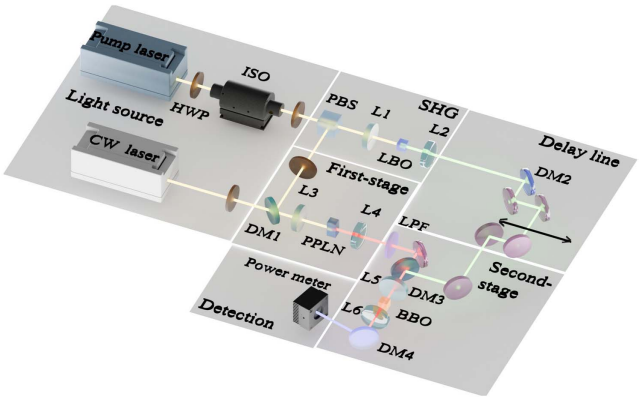

Fig. 1. Schematic of experimental setup. HWP, half-wave plate; PBS, polarization beam splitter; DM, dichroic mirror; LPF, long-pass filter; L, lens; ISO, optical isolator.

A fraction of the power (about 24.6%) is derived to drive the first-stage OPA. Since optical parametric amplification starts from the seed, the noise characteristics of the output pulses are greatly affected by the stability of the seed. Our previous work[22] showed that the narrowband CW-seeded OPA exhibits superior RIN and timing jitter performance. Therefore, this system adopts the CW source as the seed of the first-stage with an average power of 17 mW, centered at 1480 nm. The nonlinear crystal for the first-stage OPA is a 10.5-mm-long, 10-mm-wide, and 1-mm-thick MgO-doped periodically poled $LiNbO_3$ (MgO: PPLN), with six gratings and periods ranging from 28.3 to 31 μm. Because polarization is essential for phase matching, two HWPs are adopted to change the polarization of the pump and the CW seed, before spatial overlap. A telescope configuration (L3, $f3 = 150$ mm and L4, $f4 = 50$ mm) is utilized to reduce the spot diameter of the signal from the first stage in order to ensure mode-matching in the second-stage OPA. In addition, a long-pass filter (LPF) is used to block the spectral component of the pump from the mixed pulses before entering into the second-stage OPA.

Next, ~75.4% of the pump is used for SHG before the second-stage OPA. The pump power is up to 7.6 W, with a SHG conversion efficiency of 50%, delivering a power of 3.8 W at 515 nm to pump the second-stage OPA. In this OPA configuration, a BBO crystal, under type-I phase matching (cut at $\theta = 22.3°$ and $\varphi = 0°$) with thicknesses of 3 mm, is utilized as the parametric gain crystal. To realize the NIR-I region output, we employ the green light as the pump, and the signal located in 1480 nm is defined as the idler. A dichroic mirror (DM3) combines the SHG pump and idler pulses, while the optimum time overlap is achieved by adjusting the optical delay line. In order to obtain a stronger nonlinear interaction, a short focal length lens (L5, $f5 = 50$ mm) is adopted to improve the power density of the SHG pump.

3. Results and Discussion

By precisely adjusting the spatial position of the pump and CW seed, the maximum output power of 548 mW is achieved with a

pump power at 2.83 W at the first stage, while the slope efficiency was approximately 34.8%. Figure 2(a) shows the spectrum of the amplified signal light and CW seed. After amplification, the center wavelength of the signal is slightly shifted to the longer wavelength relative to that of the CW seed. Nevertheless, considering the pump is provided by a femtosecond laser, the seeded signal laser is further modulated by a femtosecond pump laser, which here serves as a broad bandwidth optical modulator. Therefore, the amplified signal also presents a short optical pulse, corresponding to a broadband spectrum. The dependency of the average signal power on the incident pump power is shown in Fig. 2(b). The pump power and signal power approximately satisfy the linear relationship. To ensure excellent spot quality, the first-stage pump power was set at 2.48 W, producing a signal power of 414 mW, and only 380 mW participate in the secondary parametric amplification due to reflection loss.

Undergoing secondary amplification, this cascaded OPA generates 347 mW second-stage signal pulses centered at 792 nm under the SHG pump power of 3.8 W. The spectrum of the second-stage signal, measured with an optical analyzer (Ocean Optics HR2000), is shown on a linear scale in Fig. 3(a). The output spectrum, which has a full-width at half-maximum (FWHM) bandwidth of 6.26 nm, is free from the CW light spectrum. Figure 3(b) shows the autocorrelation traces of the second-stage signal pulse, which reveals a 171 fs pulse duration (Gaussian fit) and is larger than that of the Fourier-transform-limited pulse duration of 147 fs. This is mainly due to group velocity dispersion accumulated in crystals, lenses, and neutral density filters (not represented) used before the autocorrelator.

To demonstrate the performance of the high-repetition-rate second-stage OPA output, we experimentally measure the dependence of the output power and pulse duration of the

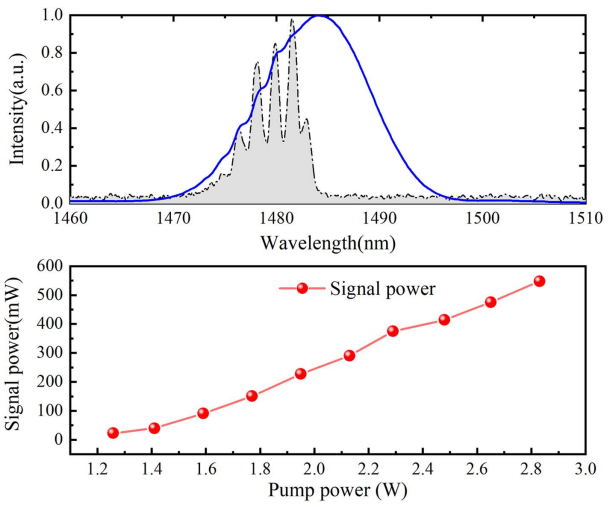

Fig. 2. (a) Measured spectrum of the amplified signal light. The shaded part under the black dash-dotted line represents the spectrum of the CW seed, and the blue solid curve represents the amplified signal light. (b) The dependence of the signal power on the pump power.

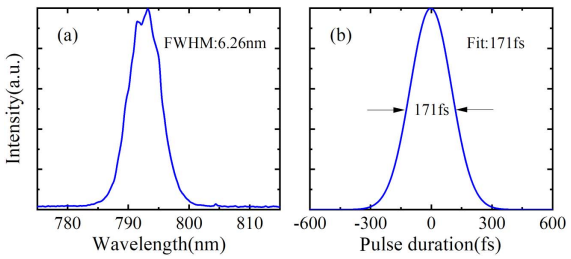

Fig. 3. Measured spectra of the second-stage signal light and the measured pulse duration.

second-stage signal light on the SHG pump and idler light (energy losses at plano-convex lenses, facets of the crystal, and DM3 have been taken into account). Reducing the idler power, while fixing the pump power at 3.8 W, the measured results demonstrate a linear relationship between the idler power and the second-stage signal power, and the pulse duration shows a similar performance, as shown in Fig. 4(a). Due to the higher power density of the idler, the nonlinear interaction between the idler and the pump occurs further forward in the BBO, resulting in more group velocity dispersion and broadening pulse duration. In a second set of measurements, reducing the pump power (an initial power of 3.8 W) step by step with the idler power fixed at 380 mW, we can see that the power of the pump and that of the signal approximately satisfy the exponential relationship, while the signal pulse duration fluctuates around 170 fs. It can be seen that the cascaded OPA does not reach the saturation station, and the signal power can be further improved by increasing the idler power and pump power. In addition, by comparing the two power curves in Figs. 4(a)

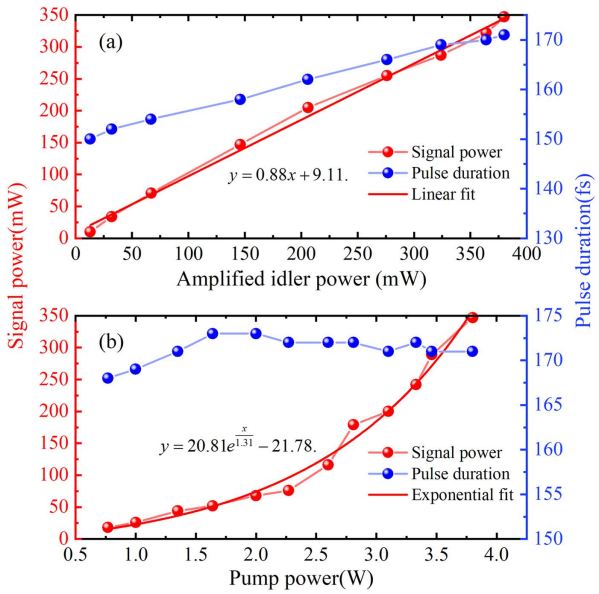

Fig. 4. The dependence of the output power and pulse duration of the second-stage signal light on (a) the idler power with the pump power fixed at 3.8 W and (b) the pump power with the idler power fixed at 380 mW.

and 4(b), it can be seen that the intensity of the nonlinear process is mainly affected by the pump powers.

A femtosecond laser has a narrower pulse duration and a wider spectrum, so it is greatly affected by the group velocity mismatch between the injection pulses. To this end, we realize that the center wavelength varies from 790 to 799 nm by slightly adjusting the optical delay line between the pump and the idler. Figure 5 plots the measured second-stage signal spectra [Fig. 5(a)], average power, and pulse duration [Fig. 5(b)] generated from the second stage OPA. At over 90% of the wavelength tuning range, the output powers exceed 150 mW and the pulse duration ranges from 160 to 170 fs. The maximum second-stage signal power is 347 mW at 792 nm, and the shortest pulse duration is 110 fs at 799 nm. During this wavelength tuning range, the power and pulse width of the second-stage signal light exhibit similar trends.

The precision and sensitivity of detecting weak signals are significantly impacted by noise, and hence, in practical applications, laser sources are expected to meet high standards for intensity noise and long-term power stability. Therefore, we built a RIN measurement system. The system's sampling rate is 5 MHz, and three time series of signals collected over 30 s are stored on a data acquisition card. We then use Fourier transform spectral analysis to process these time series to obtain the power spectral density and relative intensity noise. The RIN measurement setup is based on photodetection and spectrum analysis[23], as displayed in Fig. 6(a). The time trains of all the measured pulses are initially detected by a commercially available amplified photodiode (APD, Thorlabs PDA36A). This ADP, which is a Si PIN photodiode with an operating range of 350 to 1100 nm, has the following specifications: a risetime of 35 ns, a bandwidth of 10 MHz, and a responsivity of 0.5 A/W. A neutral density filter is placed between the APD and laser source to reduce the power below the damage threshold of the APD. Then, the photo-detected error signal passes

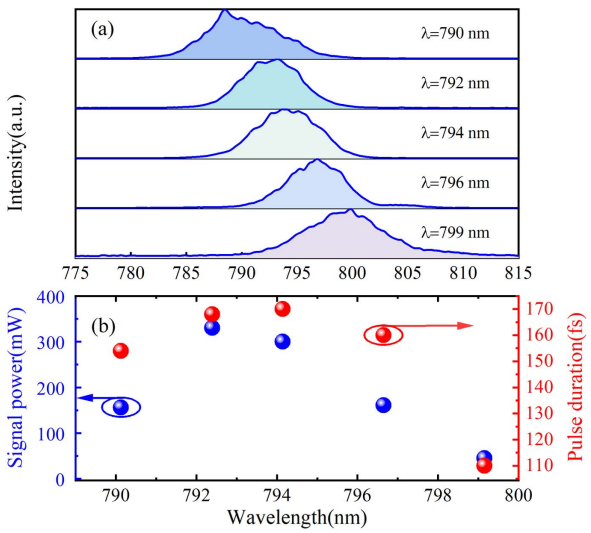

Fig. 5. (a) Measured spectra in the range of 790–799 nm and (b) the average power and pulse duration of the second-stage signal light.

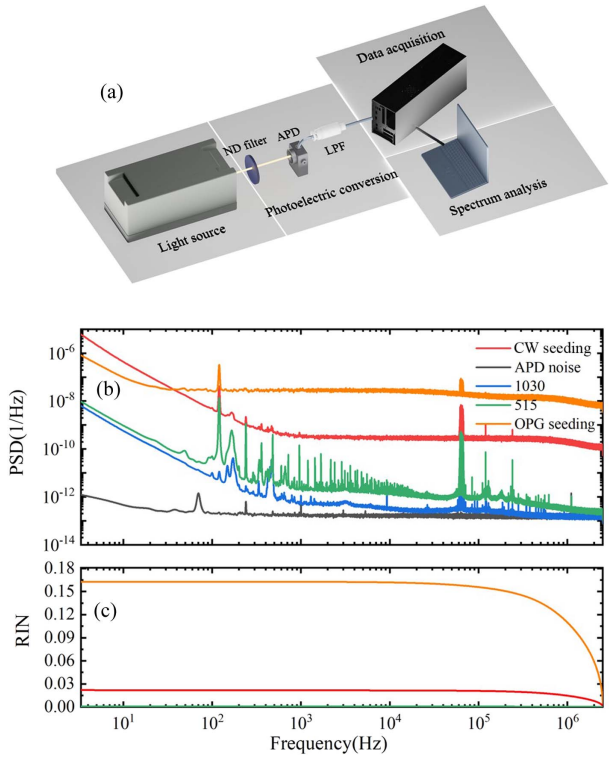

Fig. 6. (a) Setup of RIN measurement. (b) The power spectral density (PSD) and (c) the relative intensity noise (RIN) of the CW seeding signal (red), the APD noise (gray), the 1030 nm Yb-doped pump (blue), the 515 nm SHG (green), and the OPG seeding signal (orange).

through a low-pass filter with a 5 MHz cutoff frequency. After low-pass filtering, the converted electrical data is acquired by an NI LABVIEW-embedded controller (PXIE-8135) combined with the data acquisition card (PXIE-5122, bandwidth 100 MHz; risetime 3.5 ns; maximum sample rate 100 MS/s). Finally, the standard deviation and mean value of the array are used to calculate the RIN of the pulse train in the frequency domain. Guided by Ref. [24], the APD converts the optical signal to an electrical one, transforming the time-domain pulse fluctuations to the frequency domain, where both the RIN and cumulative RIN of the laser source are calculated. By comparison, we also record the RIN performance of the APD background noise, the fundamental pump, and the green light. The RMS RIN for the CW seed is 2.2%, integrated over the frequency range from 3.3 Hz to 2.5 MHz, as illustrated in Fig. 6(c). The seed laser diode plays a major role in improving the noise performance of the system. The cumulative relative intensity noise of the system without the CW seed is calculated to be 16.3%, which is ~7.4 times larger than that with the CW seed.

Figure 6(b) demonstrates that the noise at the low frequency part is mainly the 1/f noise of the fiber laser. In Fig. 6(b), three series of harmonic peaks are identified in our RIN data: peaks at 50 and 100 Hz from the power grid, harmonics at 60 and 120 Hz likely caused by a neighboring lab's strong currents, and harmonics at 65 kHz generated by the pump diode's switching power supply. In addition, in the middle-frequency band

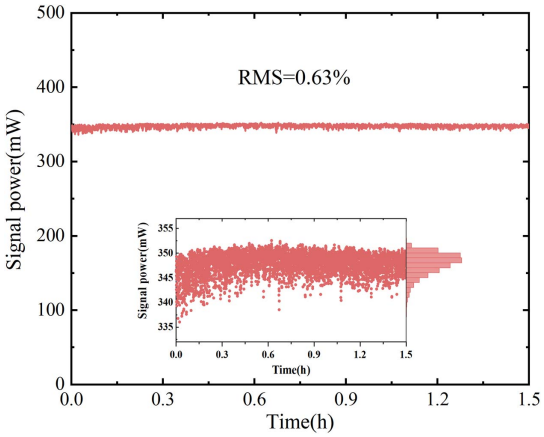

Fig. 7. Long-term power stability of the signal power at 792 nm.

(1 KHz-MHz), noise remains constant, conforming to the characteristics of white noise. Moreover, the high-frequency noise caused by quantum noise, contributes mostly to the RIN. Additionally, there is a slight drift of the RIN level of the second-stage signal light and SHG from the initial sampling frequency to around 100 Hz, caused by external mechanical vibration. As can be seen from Fig. 6, the RIN of the second-stage signal is higher than that of the pump, which can be ascribed to the large fluctuation and bandwidth of the seed source. By employing a narrow linewidth CW injection laser source, the RIN should be further reduced.

The long-term stability of the generated second-stage signal is also presented in Fig. 7. The signal power fluctuates around 345 mW at 792 nm with an RMS deviation of 0.63% over the course of 90 min. This measured result indicates that no thermal dephasing occurs in the BBO at room temperature. The stability of our entire system is subject to the external environment, such as temperature, humidity, airflow, and mechanical vibration. Indeed, the power stability can be further enhanced by integrating water cooling to regulate the crystal temperature and packaging the system to minimize external interference.

Finally, we measure the M^2 value and beam profile of the output second-stage signal using BeamSquared and infrared camera, respectively. The output beam quality is excellent, and it is an ellipse beam profile with an M^2 value of 1.11×1.29, as shown in Fig. 8. The optical films on the lenses of the infrared camera bring about the interference of the incident signal light, for which a low-pass filter is used to process the beam profile. The lens groups in the system cause astigmatism, resulting in a malposition between the waist positions in the X- and Y-directions. The different beam divergence of the two directions is caused not only by the walk-off between the pump light and the idler but also by the collimation error of the pump and the idler. Therefore, the nonlinear strength in the X- and Y-direction s is different and causes the dissimilarity of M^2 in the two directions.

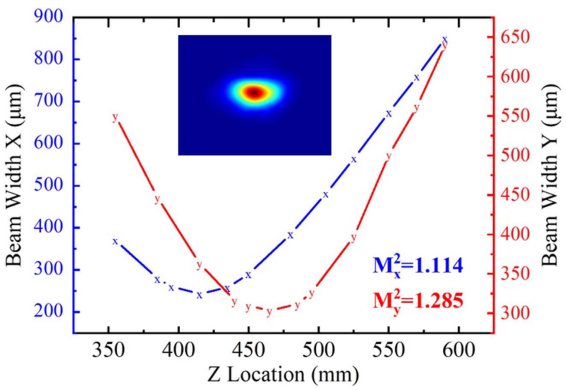

Fig. 8. M^2 measurement of the second-stage output signal light. The blue X are the horizontal beam radii and the red Y are the vertical beam radii.

4. Conclusion

In conclusion, we demonstrated a cascaded NIR-I spectrum OPA system operating at ~50 MHz and delivering an output power of up to 347 mW at 792 nm. In terms of the persistence property of the OPA, the noise performance is dominated by the CW-seed laser source. To this end, the OPA exhibits an RMS RIN of 2.2%, a long-term power stability of 0.63% RMS, and an M^2 value of 1.11×1.29. To the best of our knowledge, this is the first demonstration of the OPA working in the NIR-I spectral region initially seeded by a CW laser. The output power can be readily scaled up by elevating the pump power and the idler power. The output wavelength can be further broadened by tuning the emission wavelength of the CW laser. By utilizing a much narrower bandwidth CW laser, the noise performance can also be improved. This work opens the door to much more stable and low-noise NIR-I spectral region OPAs with a MHz high repetition rate and has the potential for application in weak signal detection and stable optical frequency comb sources.

Acknowledgements

This work was supported by the National Key R&D Program of China (No. 2023YFB3611000) and the National Natural Science Foundation of China (Nos. 62105237 and 62227821).

References

1. S. H. Chung and E. Mazur, "Surgical applications of femtosecond lasers," J. Biophotonics **2**, 557 (2009).
2. A. Tátila-Ferreira, G. A. Garcia, L. M. B. dos Santos, *et al.*, "Near infrared spectroscopy accurately detects Trypanosoma cruzi non-destructively in midguts, rectum and excreta samples of Triatoma infestans," Sci. Rep. **11**, 23884 (2021).
3. T. Meunier and A. Weck, "Fabrication of microlens arrays in polycarbonate with nanojoule energy femtosecond laser pulses," in *Conference on Lasers and Electro-Optics (CLEO)* (2012).
4. Y. L. Zhang, L. Guo, S. Wei, *et al.*, "Direct imprinting of microcircuits on graphene oxides film by femtosecond laser reduction," Nano Today **5**, 15 (2010).
5. G. Sansone, F. Calegari, and M. Nisoli, "Attosecond technology and science," IEEE J. Sel. Top. Quantum Electron. **18**, 507 (2012).

6. R. Ell, U. Morgner, F. X. Kärtner, *et al.*, "Generation of 5-fs pulses and octave-spanning spectra directly from a Ti:sapphire laser," Opt. Lett. **26**, 373 (2001).
7. M. Nisoli, S. De Silvestri, O. Svelto, *et al.*, "Compression of high-energy laser pulses below 5 fs," Opt. Lett. **22**, 522 (1997).
8. I. D. Jung, F. X. Kärtner, N. Matuschek, *et al.*, "Self-starting 6.5-fs pulses from a Ti:sapphire laser," Opt. Lett. **22**, 1009 (1997).
9. J. Seres, A. Müller, E. Seres, *et al.*, "Sub-10-fs, terawatt-scale Ti:sapphire laser system," Opt. Lett. **28**, 1832 (2003).
10. N. Coluccelli, D. Viola, V. Kumar, *et al.*, "Tunable 30 fs light pulses at 1 W power level from a Yb-pumped optical parametric oscillator," Opt. Lett. **42**, 4545 (2017).
11. K. Nagashima, R. Itakura, and N. Ishii, "Broadband operation of a synchronously pumped optical parametric oscillator with a spatially dispersed beam," Opt. Lett. **46**, 4414 (2021).
12. C. W. Rudy, A. Marandi, K. A. Ingold, *et al.*, "Sub-50 fs pulses around 2070 nm from a synchronously-pumped, degenerate OPO," Opt. Express **20**, 27589 (2012).
13. I. Pipinytė, J. Vengelis, V. Jarutis, *et al.*, "Investigation of continuum generation in the non-zero dispersion-shifted fiber pumped by femtosecond nanojoule pulses in 1450–1800 nm spectral range," Results Phys. **17**, 103064 (2020).
14. S. Cialdi, E. Suerra, M. G. A. Paris, *et al.*, "Technique for active stabilization of the relative phase between seed and pump in an optical parametric oscillator," Phys. Rev. A **104**, 053706 (2021).
15. M. Heurs, I. R. Petersen, M. R. James, *et al.*, "Homodyne locking of a squeezer," Opt. Lett. **34**, 2465 (2009).
16. Y. Li, Y. Leng, W. Li, *et al.*, "Broadband 800nm pulse generation with an optical parametric amplifier based on BiB3O6," in *Conference on Lasers and Electro-Optics Pacific Rim* (2015), paper 25C1_2.
17. T. Deckert, A. Vanderhaegen, and D. Brida, "Sub-8-fs pulses in the visible to near-infrared by a degenerate optical parametric amplifier," Opt. Lett. **48**, 4496 (2023).
18. A. M. Siddiqui, G. Cirmi, D. Brida, *et al.*, "Generation of <7 fs pulses at 800 nm from a blue-pumped optical parametric amplifier at degeneracy," Opt. Lett. **34**, 3592 (2009).
19. H. Pires, J. Alves, V. Hariton, *et al.*, "Ultrabroadband OPA in YCOB with a sub-ps pump source," Photonics **10**, 253 (2023).
20. W. Chen, J. Fan, A. Ge, *et al.*, "Intensity and temporal noise characteristics in femtosecond optical parametric amplifiers," Opt. Express **25**, 31263 (2017).
21. K.-Y. Wang and A. C. Foster, "GHz near-IR optical parametric amplifier using a hydrogenated amorphous silicon waveguide," in *CLEO: 2014, OSA Technical Digest (online)* (2014), paper SW3I.7.
22. T. Steinle, V. Kumar, A. Steinmann, *et al.*, "Compact, low-noise, all-solid-state laser system for stimulated Raman scattering microscopy," Opt. Lett. **40**, 593 (2015).
23. C. R. Smith, R. D. Engelsholm, and O. Bang, "Pulse-to-pulse relative intensity noise measurements for ultrafast lasers," Opt. Express **30**, 8136 (2022).
24. K. Petermann, *Laser Diode Modulation and Noise* (Springer Science & Business Media, 2012).